01 Jun 2021

A Gallium-Doped Cement for the Treatment of Bone Cancers. the Effect of ZnO ↔ Ga2O3substitution of an Ionomeric Glass Series on the Rheological, Mechanical, PH and Ion-Eluting Properties of their Corresponding Glass Polyalkenoate Cements

Sunjeev Phull

Alireza Rahimnejad Yazdi

Mark R. Towler
Missouri University of Science and Technology, mtowler@mst.edu

Recommended Citation

PAPER • OPEN ACCESS

A Gallium-doped cement for the treatment of bone cancers. The effect of ZnO ↔ Ga_2O_3 substitution of an ionomeric glass series on the rheological, mechanical, pH and ion-eluting properties of their corresponding glass polyalkenoate cements

To cite this article: Sunjeev Phull *et al* 2021 *Mater. Res. Express* **8** 065401

View the article online for updates and enhancements.

Materials Research Express

PAPER

A Gallium-doped cement for the treatment of bone cancers. The effect of ZnO ↔ Ga$_2$O$_3$ substitution of an ionomeric glass series on the rheological, mechanical, pH and ion-eluting properties of their corresponding glass polyalkenoate cements

Sunjeev Phull[1,2] , Alireza Rahimnejad Yazdi[1,2] and Mark R Towler[1,2]

[1] Li Ka Shing Knowledge Institute, St. Michael's Hospital, Toronto M5B 1W8, Ontario, Canada
[2] Department of Mechanical Engineering, Ryerson University, Toronto M5B 2K3, Ontario, Canada

E-mail: mtowler@ryerson.ca

Abstract

The primary treatment for patients suffering from bone cancers is resection of the tumour followed by reconstruction of the damaged bone. Despite the administration of post-operative chemotherapy, tumour recurrence continues to present itself as a severe complication leading to re-operation. Attempts to incorporate chemotherapeutic drugs into bone cements elicits local toxic effects on healthy bone, which could compromise implant fixation. Alternatively, the local administration of gallium (Ga) may prove to be more effective. This report considers the development of a Ga ionomeric glass series ($0.48SiO_2$-$0.355ZnO$-$0.06CaO$-$0.08SrO$-$0.02P_2O_5$-$0.005Ta_2O_5$, with 0.01–0.05 mol% substitution for ZnO). X-ray Diffraction (XRD) confirmed the amorphous glass structure and Energy Dispersive x-ray Fluorescence (EDXRF) verified the successful addition of Ga into the glass series at the expense of Zinc (Zn). A Ga-GPC series was then formulated by mixing the glass particles with aqueous poly(acrylic) acid (PAA) and trisodium citrate (TSC). Fourier transform infrared (FTIR) spectroscopy demonstrated no structural changes to the GPC matrix with the incorporation of Ga. Measurements of the rheological properties demonstrated an exponential increase in setting time with increasing Ga content. Furthermore, the addition of ⩾3 mol% Ga demonstrated deleterious effects on the GPC's mechanical properties and an analysis of pH confirmed that it decreased with increasing Ga content, suggesting a reduction in glass reactivity and PAA cross-linking. Finally, inductively coupled plasma—optical emission spectrometry (ICP-OES) demonstrated the controlled release of Ga across the GPC series, which will prove beneficial to future *in vitro* studies.

1. Introduction

Primary bone cancers are rare and account for less than 0.2% of all cancers [1, 2], while the incidence of metastatic bone lesions are common among patients with advanced cancers: 65%–75% in the breast, 65%–75% in prostate, 60% thyroid, 30%–40% in the lung and 40% in bladder [3]. The predominant treatment for both primary and severe metastatic bone cancers is reconstruction surgery [4, 5]. Various materials have been implemented for bone reconstruction, including allografts, autografts, osteosynthetic implants and endoprostheses. Unfortunately, such materials are susceptible to serious complications that can lead to implant failure, including infection (up to 11.7% of implantations), aseptic loosening (up to 12.5%) and mechanical failure (up to 14.7%) [6–12]. Clinical case studies in the metastatic bone cancer population have demonstrated that the use of poly (methylmethacrylate) (PMMA) bone cement reduced the rate of post-surgical complications when compared to traditional non-cemented methods (press-fitting/locking) [13–15]; nevertheless, the use of PMMA has not addressed the occurrence of either infection or aseptic loosening [16]. For instance, Benevenia *et al* reported a 21% versus 33% complication rate when comparing cemented and non-cemented

endoprostheses, respectively [14]. Furthermore, despite resection of the tumour and consequent chemotherapy, tumour recurrence continues to present itself as a prevalent issue leading to the need for reoperation (3.1%–14.7%) [6–12, 16–19]. Hence, innovation is required not only to reduce the rate of complications but also to improve the effectiveness of chemotherapy.

Inspired by the incorporation of antibiotics into bone cement, researchers have investigated the employment of PMMA bone cement as a local antineoplastic drug (ANPD) carrier; however, these drugs have low therapeutic indices and demonstrable risks around bone necrosis and possible loss of implant fixation [20–24]. Furthermore, although PMMA bone cement is the gold standard for orthopedic fixation, it possesses a native arsenal of cytotoxic effects (thermal necrosis, monomer toxicity and periprosthetic osteolysis) and is bioinert, thus presenting the opportunity to investigate new materials to repair bones damaged by cancer [20]. Alternatively, inorganic bone cements, including calcium phosphate cements (CPCs) and glass polyalkenoate cements (GPCs), have also been investigated as local ANPD carriers as it was hypothesized that their biological properties might oppose the toxic nature of these drugs and support osteogenesis [25–32]. Unfortunately, studies on ANPD-loaded CPCs demonstrated similar cytotoxic effects on healthy bone [27, 31]; moreover, the use of resorbable calcium phosphate poses a contradiction, as its introduction to a lytic area, such as metastatic bone lesions, poses the risk of initiating or aggravating hypercalcemia. Furthermore, an ANPD-loaded GPC showed cytotoxic effects on NIH-3T3 mouse fibroblasts [32]. The current knowledge of chemotherapeutic bone cements demonstrates that, regardless of cement type, ANPD toxicity is inevitable and alternative chemotherapeutic agents should be investigated [20].

Hart *et al* [33] studied the antitumour activity of the salts of inorganic group IIIa metals, concluding that Ga nitrate had the potential for clinical usefulness in treating solid tumours. Furthermore, several studies have noted the synergistic interactions of Ga nitrate with chemotherapeutic drugs [34–37]. In-depth studies into its anti-cancer role have demonstrated the effect of Ga on the cellular iron metabolism, resulting in the inhibition of ribonucleotide reductase formation, an enzyme responsible for the formation of deoxyribonucleotides [38–40]; therefore, halting DNA synthesis and the proliferation of rapidly dividing (malignant) cells. Ga has also been found to inhibit calcium resorption [41, 42]. Studies by Warrell *et al* [43] and Cvitkovic *et al* [44] demonstrated that Ga nitrate is superior to bisphosphates for inhibiting bone resorption. Furthermore, Ga nitrate is FDA-approved for the treatment of cancer-related hypercalcemia [45]. Therefore, the local administration of Ga by a GPC may prove beneficial to the treatment of such patients.

GPCs have been used in both restorative and orthodontic dentistry for over 40 years and in ear, nose and throat surgery for over 20 years [46–48]; however, the presence of aluminum (Al) in the glass phase of such GPCs have inhibited their translation to orthopedic applications [49, 50], resulting in the recent development of Al-free GPCs [51–60]. GPCs are set by an isothermic neutralization reaction between a silicate-based ionomeric glass and aqueous poly (acrylic acid) (PAA). When mixed, the free PAA protons attack the glass particles and liberate cations, which then cross-link the PAA chains, resulting in a polysalt matrix reinforced by reacted and unreacted glass particles [61]. GPCs are considered bioactive due to their release of therapeutic ions loaded into the cement's glass phase [62, 63]. Furthermore, two studies have investigated the incorporation of gallium (Ga) into GPC compositions [59, 60], demonstrating the effects on the structural properties of their base ionomer silicate glass, as well as the rheologic, mechanical and ion eluting properties of the corresponding GPCs. While considerable amounts of Ga were incorporated (dopant levels of 8 and 16 mol%), these GPCs were only able to elute up to 3 parts per million (ppm) of Ga^{3+}, and no attempts were made to investigate the chemotherapeutic potential or cytotoxic effects of these cements *in vitro* [59].

In previous studies on a related glass series, Alhalawani and colleagues developed a novel SiO_2-ZnO-CaO-SrO-P_2O_5-Ta_2O_5 based GPC for wrist fracture fixation [53, 54, 64]. The purpose of this current body of work is to expand on this and incorporate variable amounts of Ga (0–5 mol%), at the expense of zinc (Zn), into the glass phase of these GPCs to tailor them for the treatment of bone cancers. Specifically, this study aims to understand further the role of Ga incorporation on the GPC setting chemistry, pH and their rheological, mechanical and ion release properties.

2. Materials and methods

2.1. Glass synthesis and cement preparation

Six Ga containing ionomeric glass compositions were formulated (table 1). C-TA0 represents the Ga-free (control) glass, while the remaining glasses (C-TA1 through C-TA5) varied from 1–5 mol% Ga, substituted at the expense of Zn. Calculated amounts of the glass precursor, analytical grade reagents (Fisher Scientific, Ottawa, and Sigma-Aldrich, Oakville, both Canada) were weighed out and thoroughly mixed in a glass beaker. The mix was then placed in a platinum crucible and fired in a furnace (Zircar Hot Spot 110, Florida, New York, USA) at 1650 °C for 1.5 h. Molten glass was shock quenched into water at room temperature (~23 °C), and the

Table 1. Glass compositions (expressed as mole fractions).

	SiO_2	ZnO	CaO	SrO	P_2O_5	Ta_2O_5	Ga_2O_3
C-TA0	0.48	0.355	0.06	0.08	0.02	0.005	0
C-TA1	0.48	0.345	0.06	0.08	0.02	0.005	0.01
C-TA2	0.48	0.335	0.06	0.08	0.02	0.005	0.02
C-TA3	0.48	0.325	0.06	0.08	0.02	0.005	0.03
C-TA4	0.48	0.315	0.06	0.08	0.02	0.005	0.04
C-TA5	0.48	0.305	0.06	0.08	0.02	0.005	0.05

obtained glass frit was dried in an incubator (37 °C) for 24 h. The dried glass frit was ball milled and sieved to a maximum particle size of 45 μm. Glass powder was annealed by reaching the temperature of 640 °C over 3 h, remaining at the temperature for 12 h, and returning to room temperature over a further 3 h (total, 16 h). Annealing was performed to reduce glass reactivity (relieve internal stresses) and achieve longer GPC working times

GPC samples were prepared by thoroughly mixing a ratio of 1 g glass powders, 0.4 g PAA (PAA35, Mw = 55 000, Advanced Healthcare Ltd), 0.6 ml deionized (DI) water and 0.1 g tri-sodium citrate (TSC) (Sigma-Aldrich, Oakville, Canada). Briefly, PAA and TSC were mixed with DI water until they had completely dissolved. This aqueous gel was mixed in room temperature (23 ± 1 °C) with the glass powder to obtain the final GPC.

2.2. X-ray diffraction (XRD)
XRD diffraction patterns of the glass powders were collected using a multipurpose x-ray diffractometer (Malvern Panalytical, Malvern, Worcestershire, UK) with a Cu source, from 10 to 90°, at a scan step size 0.1°, using a generator voltage of 45 kV and a tube current of 40 mA.

2.3. Energy dispersive x-ray fluorescence (EDXRF)
EDXRF spectra of the glass powers were obtained using an Epsilon 4 Food and environment EDXRF Spectrometer (Malvern Panalytical, Malvern, Worcestershire, UK) under four different excitation conditions including: using a silver filter with tube voltage of 50 kV, a copper filter with a tube voltage of 50 kV, an aluminum filter with a tube voltage of 12 kV and no filter with a tube voltage of 10 kV. Qualitative analysis was performed to identify the elements present in the sample, and quantitative analysis was performed to obtain the %mass of each identified element. Both quantitative and qualitative analyses were carried out using the Omnian XRF analysis program (Malvern Panalytical, Malvern, Worcestershire, UK).

2.4. Rheological properties
The rheological properties (n = 3) of the GPCs were recorded at room temperature (23 ± 1 °C) using a stopwatch. Working times (Tw) were defined as the time from the start of mixing to when the materials began to exhibit elastic properties. The net setting times (Ts) were determined in accordance with ISO 9917:2007 [65]. Briefly, a mold (7 mm length, 8 mm width and 5 mm height) was filled to the surface with liquid GPC. An indenter (mass = 400 g, diameter = 1.06 mm) was lowered on the GPCs and was allowed to rest for 5 s. If an indentation was formed on the GPC, then the needle was repositioned to a clean (non-indented) area, and the process was repeated. Ts was determined once no indentation was visible to the naked eye.

2.5. Fourier transform infrared (FTIR) spectroscopy
Cement cylinders (diameter, 4 mm & height, 6 mm) were prepared by filling a stainless-steel mold with freshly mixed cement. The mold was then sandwiched between two stainless-steel plates lined with acetate sheets and incubated at 37 °C for 100 min. Samples were then immersed in 10 ml of DI water (37 °C) and aged for either 1, 7 or 30-days. At the time of testing, samples were ground using a mortar and pestle and FTIR spectra were collected in ambient air (23 ± 1 °C) using a Cary 630 FTIR Spectrometer (Agilent Technologies, Santa Clara, CA, USA) via the total reflectance technique with a ZnSe crystal. The analysis was performed in the wavenumbers ranging from 4000 to 650 cm^{-1} with a spectral resolution of 4 cm^{-1}.

2.6. Determination of mechanical properties
2.6.1. Determination of compressive strength and Young's modulus
The compressive strengths of the six GPCs were determined in accordance with ISO 9917:2007 [65]. Briefly, cement cylinders (diameter, 4 mm & height, 6 mm) were prepared and aged in 10 ml of DI water (37 °C) and aged for either 1, 7 or 30-days (n = 5). The samples were tested in ambient air (23 ± 1 °C) using an Instron 5966 universal Testing Machine (Instron Corp., Norwood, MA, USA) fitted with a ±10 kN load cell with a crosshead

speed of 1 mm min^{-1}. The compressive strength (σ_c) of each sample was calculated using equation (1) (equation (1)):

$$\sigma_c = \frac{4p}{\pi d^2} \tag{1}$$

where, p is the sample failure load (N) sample and d is the sample diameter (mm).

The Young's modulus of each GPC was obtained from the elastic region of the stress-strain curves that were collected during the determination of compressive strength.

2.6.2. Determination of biaxial flexural strength

The biaxial flexural strengths of the six GPCs were determined in accordance with the method described by Williams *et al* [66]. Cement discs (16 mm diameter and 2 mm thick) were prepared by filling silicon rubber molds with freshly mixed cement. The mold was then sandwiched between two stainless-steel plates lined with acetate sheets and incubated at 37 °C for 100 min. Samples were then placed in 10 ml of DI water (37 °C) and aged for either 1, 7 or 30-days (n = 5).

The cement discs were tested in ambient air (23 ± 1 °C) using the same universal Testing Machine described in section 2.6.2. with a crosshead speed of 1 mm min^{-1}. The discs were centered on a three-ball bearing support, and the load was applied as a point to the center of the disc. The biaxial flexural strength (σ_b) was calculated by the following relation:

$$\sigma_b = \frac{F}{t^2}\left(0.63 \ln\left(\frac{a}{t}\right) + 1.156\right) \tag{2}$$

where, F is the sample failure load (N), t is the sample thickness (mm) and a is the radius of the support diameter (3.825 mm).

2.7. pH analysis

The effect of Ga incorporation on the pH of the GPC series was measured in ambient conditions (23 ± 1 °C) using an Orion VersaStar Pro pH Benchtop Meter (Thermo Fisher Scientific, Waltham, MA) equipped with a flat membrane microelectrode (MI-406, Microelectrodes, Bedford, NH) and a rate reference electrode (MI-041, Microelectrodes). Cement cylinders (diameter, 4 mm; height, 6 mm) were prepared and aged in 10 ml of DI water at 37 °C for 1, 7 and 30-days (n = 3). Prior to testing, the pH meter was calibrated using pH buffer solution 4.00 ± 0.02 and 7.00 ± 0.02 (Thermo Fisher Scientific, Waltham, MA).

2.8. Ion release

The ion release of the GPC series was measured in ambient air (23 ± 1 °C) using inductively coupled plasma—optical emission spectrometry (ICP-OES 5110, Agilent, Santa Clarita, CA, USA). Calibration standards (0, 1, 5, 10 and 30 ppm) were prepared from 1000 ppm stock solutions (Sigma-Aldrich, Oakville, Canada) for the glass composition elements. Cement cylinders were aged in 10 ml of DI water at 37 °C and tested after 1, 7 and 30-days (n = 5).

2.9. Statistical analysis

Statistical analysis was performed using Prism GraphPad 9.0 (GraphPad Software. Inc., San Diego, CA, USA). The Shapiro-Wilk test was used to test normality, and parametric one-way ANOVA was used to analyze all data, with the Tukey's test for multiple comparisons. Results were considered statistically significant when p values were <0.05.

3. Results and discussion

3.1. X-ray diffraction (XRD)

The XRD diffraction patterns across the glass series are displayed in figure 1. It is crucial that the structure of these glasses be amorphous, as a crystalline structure, or a glass with crystalline phases, would be resistant to acid attack by the PAA. The diffuse wave in the XRD diffractogram (~20–40°) represents the amorphous silica glass structure [67]. The peak detected at ~15° may indicate a carbon-oxide species formed by the carbonate precursors used to form the glasses as Choi *et al* [68] and Huh *et al* [69] have previously assigned comparable peaks to microcrystalline cellulose and graphene oxide, respectively. Furthermore, the diffraction patterns remain consistent across the glass series, confirming that any changes observed in the GPC properties may be solely attributed to the incorporation of Ga rather than phase changes in the glass structures.
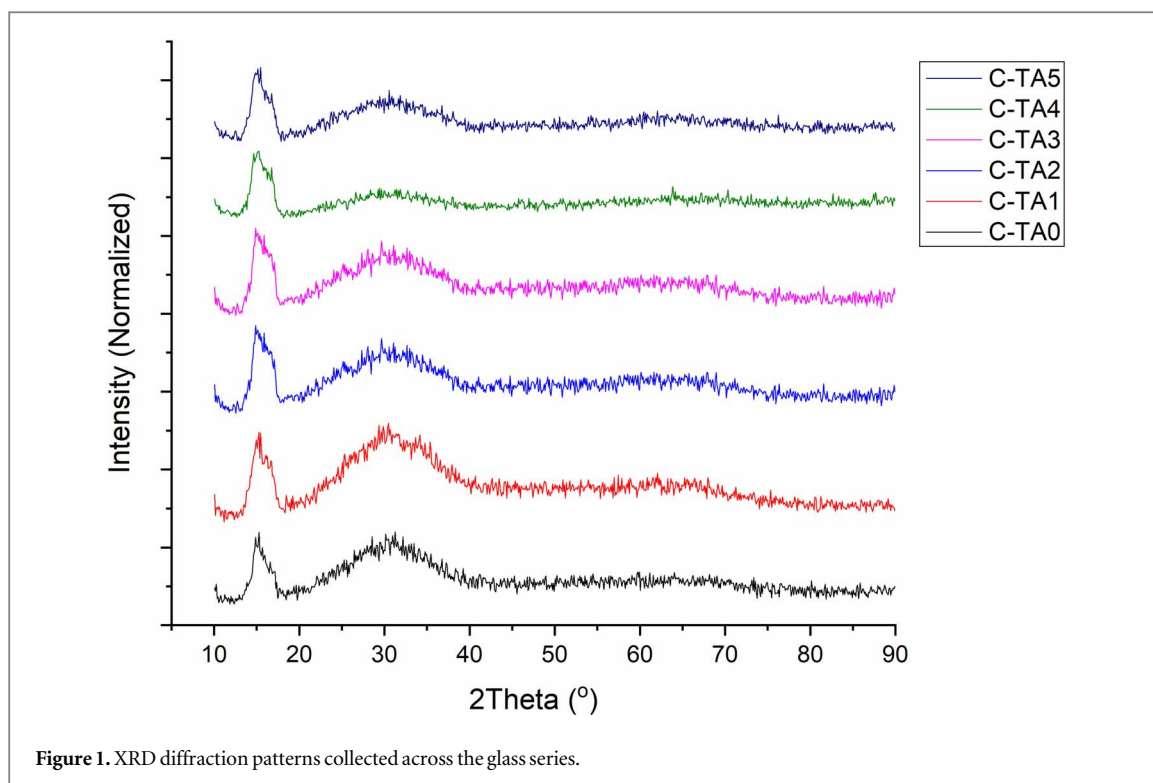
Figure 1. XRD diffraction patterns collected across the glass series.

Table 2. The calculated %mass values (theoretical concentration—T.C.) and %mass values obtained from EDXRF (experimental concentration—E.C.).

	SiO_2		ZnO		CaO		SrO		P_2O_5		Ta_2O_5		Ga_2O_3	
	T. C.	E.C.	T.C.	E.C.	T.C.	E.C.	T.C	E.C.	T.C.	E.C.	T.C.	E.C.	T.C.	E.C.
C-TA0	37.32	32.59	37.39	42.86	4.30	4.83	10.58	12.56	7.25	3.24	2.82	3.91	0.00	0.00
C-TA1	36.82	34.78	35.84	40.07	4.30	4.81	10.58	11.97	7.25	2.02	2.82	3.52	2.39	2.83
C-TA2	36.33	34.12	34.34	38.47	4.24	4.74	10.44	11.84	7.15	1.94	2.78	3.47	4.72	5.42
C-TA3	35.85	33.31	32.88	36.98	4.18	4.69	10.30	11.78	7.06	1.89	2.75	3.40	6.99	7.95
C-TA4	35.38	33.81	31.45	34.83	4.13	4.58	10.17	11.34	6.97	1.93	2.71	3.27	9.20	10.23
C-TA5	34.93	32.39	30.06	33.84	4.08	4.55	10.04	11.38	6.88	1.88	2.68	3.24	11.35	12.73

3.2. Energy dispersive x-ray fluorescence (EDXRF)

EDXRF was performed to study the elemental composition of the glass series. Table 2 compares the theoretical (calculated) %mass values with the quantitative data obtained from EDXRF. The results demonstrate the successful incorporation of Ga at the expense of Zn across the glass series (Ga increase from 0%–12.73%mass and Zn decrease from 42.86%–33.84%mass). Furthermore, slight discrepancies were observed between the theoretical and experimental concentrations of each element, the largest of which was observed for P_2O_5 (mean difference of −4.93% between the E.C. and the T.C.). Other major discrepancies (>1%) between the E.C. and T.C. include ZnO (mean difference of −4.26% mass), SrO (1.48%mass) and SiO_2 (−2.62%mass). The majority of the glass precursor reagents employed the use of the oxide or carbonate of each element (i.e., $CaCO_3$, $SrCO_3$, SiO_2 etc). However, the reactive nature of P_2O_5 has led to the use of ammonium dihydrogen phosphate $((NH_4) H_2PO_4)$ as an alternative reagent for the incorporation of phosphorus in this glass series, which may explain the observed discrepancies.

While calculating each reagent amount to add to the glass mix, a correction is required when the exact compound is not being used. For instance, no correction was required for the amount of SiO_2 since the exact element was added to the mix, while $SrCO_3$ required correction due to a discrepancy between its molecular weight (Mw) and the Mw of the compound obtained in the glass (SrO). This correction occurs by multiplying the calculated mass by the ratio of the Mw of the glass compound and the glass precursor. In the majority of cases, this ratio is above 1; however, glass precursor for P_2O_5, $(NH_4) H_2PO_4$, has a smaller Mw; therefore, the correction ratio is less than 1 and is likely to be the cause of the large discrepancy observed for P_2O_5.
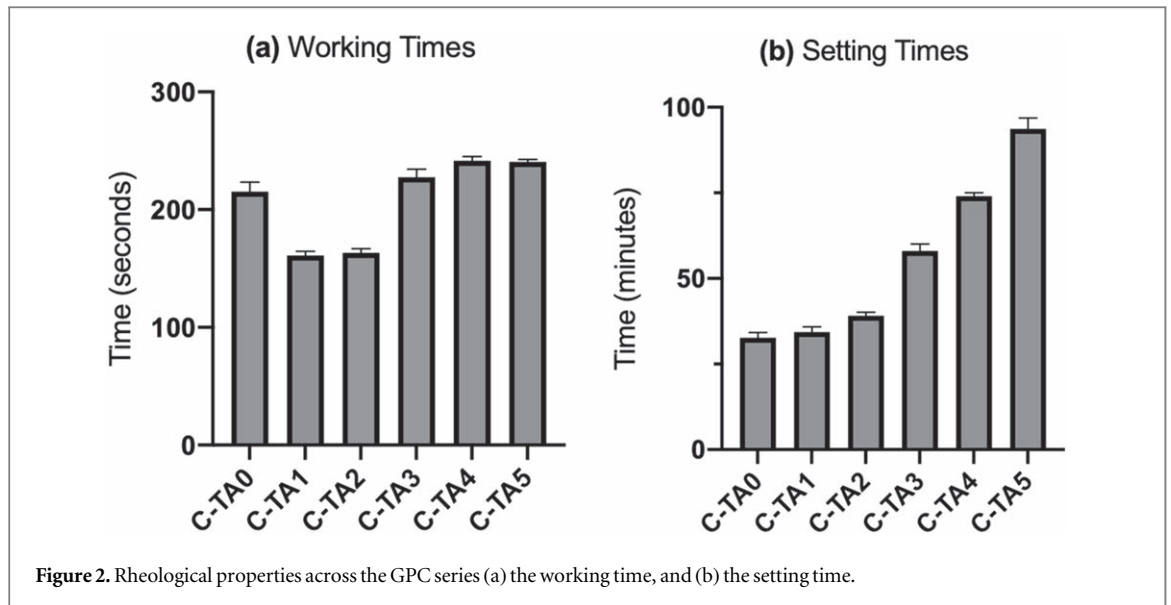
Figure 2. Rheological properties across the GPC series (a) the working time, and (b) the setting time.

3.3. Rheological properties

The rheological properties of the GPCs are of significant importance as these properties are assumed to indicate the effect of Ga incorporation on the cement's setting chemistry. Figure 2(a) presents the Tw, and figure 2(b) presents the Ts across the GPC series. C-TA1 and C-TA2 demonstrated a significantly lower Tw compared to C-TA0 ($P < 0.05$), and no differences were observed between C-TA0 and C-TA3 ($P > 0.05$). Furthermore, C-TA4 and C-TA5 demonstrated significantly higher Tw compared to C-TA0 ($P < 0.05$). The Ts demonstrated an exponential-like trend with increasing Ga content and ranged from 33–96 min. Although C-TA0 and C-TA1 demonstrated similar Ts ($P = 0.88$), the addition of $\geqslant$ 2 mol% Ga in the glass composition demonstrated significant increases in the Ts between each of the GPCs ($P < 0.05$).

These results are in agreement with previous studies conducted on Ga-incorporated GPCs [59, 60]. For instance, Wren *et al* [60] noted that Tw increased from 125–200 s and Ts increased from 150 s to >550 s with the addition of 16 mol% Ga. The substitution of Ga in place of Zn is expected to result in a more stable and electro-neutral glass structure since Ga^{3+} provides a larger number of positive charges compared to Zn^{2+}. This increase in the glass's network stability would ultimately reduce its reactivity, causing a delay in cation liberation and their consequent gelation process with the PAA carboxyl groups (COOH) and an increased Tw and Ts [53]. Furthermore, Wren *et al* [60] demonstrated that both Tw and Ts decreased by using a higher molecular weight PAA, explained by entangled polymer dynamics and reptation theory, which states that the relaxation time of long polymer chains is proportional to the cube of their molecular mass. However, the incorporation of Ga in place of Zn may also affect this relaxation time.

The Edwards tube concept describes the movement of a polymer chain to be confined to a tube, with an average diameter *a*, which is defined by the position of other polymer chains [70]. Moreover, the number of monomers in a single entanglement strand is defined as the number of Kuhn monomers, *Ne*, present in chain size length *a*, which is calculated using the following relation [70]:

$$a \approx bNe^{1/2} \tag{3}$$

where b is the Kuhn length. Furthermore, the reptation time (τ_{rep}) is described by [70]:

$$\tau_{rep} = \frac{\zeta b^2}{K_B T} Ne^2 \left(\frac{N}{Ne}\right)^2 \tag{4}$$

where ζ is the friction coefficient corresponding to each monomer unit, K_B is the Boltzmann's constant, T is the temperature, and N is the total number of monomer units in the polymer chain. By rearranging equation (3) and substituting into *b* in equation (4), the following expression is obtained [70]:

$$\tau_{rep} = \frac{\zeta a^2}{K_B T} Ne \left(\frac{N}{Ne}\right)^2 \tag{5}$$

This relation demonstrates that, τ_{rep} is proportional to the square of the average tube diameter (*a*). Ga has a larger atomic radius than Zn (187 pm and 139 pm, respectively) and a smaller difference in electronegativity with oxygen compared to Zn (1.63 and 1.79, respectively); therefore, it may be assumed that the cross-linking of Ga^{3+} and COO^- in the GPC's polysalt matrix results in a larger bond length compared to Zn cross-linking [61]. Since the tube diameter of a single polymer chain is determined by the presence of other polymer chains, this

Figure 3. FTIR spectra of GPCs after (a) 1-Day, (b) 7-Days, and (c) 30-Days of maturation in DI water.
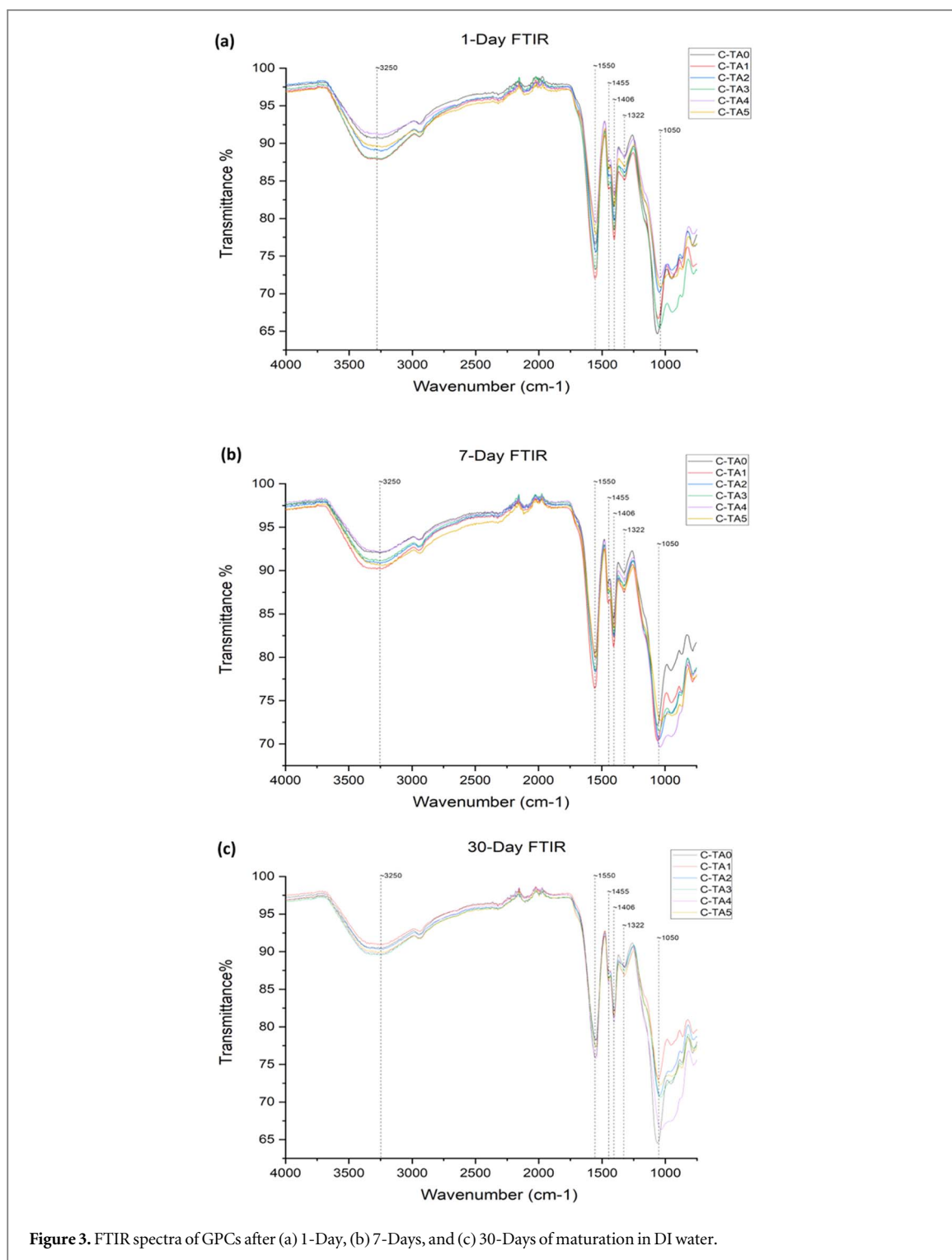
dispersion of the surrounding strands may cause an increase in its average tube diameter (*a*). Furthermore, increasing Ga content may increase Ga-COO bonding, further increasing polymer chain dispersion and the average tube diameter, resulting in a larger Ts. While this is a crude analysis of entangled polymer dynamics, it provides a possible explanation for the increase in Ts across the GPC series.

3.4. Fourier transform infrared spectroscopic (FTIR)

FTIR spectroscopy was performed to investigate the setting kinetics between the glass powder and the aqueous PAA. The FITR spectra collected for the 1, 7 and 30-day samples are displayed in figures 3(a)–(c), respectively. The broad peak centered at $\sim$3250 cm^{-1} is assigned to the O–H stretching of water [71]. The peaks centered at $\sim$1550 cm^{-1}, $\sim$1455 cm^{-1}, $\sim$1406 cm^{-1} and $\sim$1322 cm^{-1} are assigned to asymmetric/symmetrically stretching vibration of a carboxyl group bonded to cations that were liberated from the glass structure [53, 72, 73].
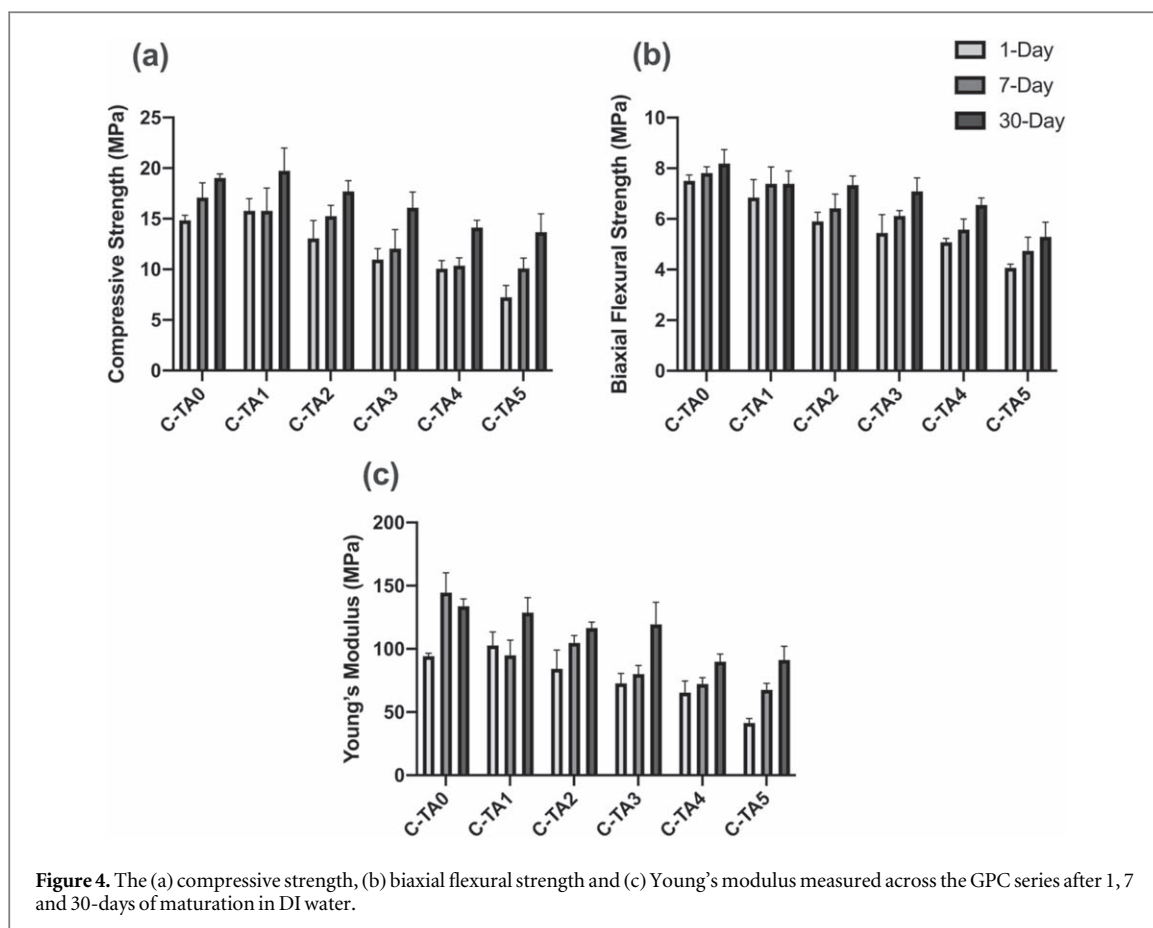
Figure 4. The (a) compressive strength, (b) biaxial flexural strength and (c) Young's modulus measured across the GPC series after 1, 7 and 30-days of maturation in DI water.

Furthermore, the peak centered at ~1050 is assigned to Si-O-Si bridges [53]. Alhalawani *et al* [59] reported the formation of a shoulder peak at ~1700 cm^{-1} in the 1-day GPCs mixed with glasses containing 8 mol% and 16 mol% Ga, which was assigned to unreacted COOH functional group of the PAA [73], and did not appear in their spectra at seven and 30-days. The presence of this shoulder peak may be related to the alterations of glass reactivity caused by the substitution of Ga for Zn, as discussed in section 3.3. The relatively high Ga doping of these glasses may have reduced their reactivity enough to result in a high presence of unreacted COOH groups that was detected by FTIR analysis of their corresponding GPCs at early maturation (1-day). In contrast, the lower Ga dopant levels in the present GPC series did not result in the detection of this peak at any time point. Moreover, the FTIR spectra do not demonstrate the evidence of any structural changes to this GPC series with the addition of 1–5 mol% Ga into the glass phase.

3.5. Mechanical properties
The compressive strength (σ_c), biaxial flexural strength (σ_b), and Young's modulus (E) of each cement tested over 1, 7 and 30 days are presented in figure 4. These mechanical properties demonstrated two trends:

(1) A global increase in mechanical properties as the cements were aged, attributed to continuous ion liberation from unreacted glass particles during GPC maturation that subsequently increases the crosslinking between PAA chains [73, 74].

(2) A general decrease in the mechanical properties with increasing Ga over the GPC series.

Figure 4(a) displays σ_c as a function of Ga content and time. The greatest σ_c was observed for C-TA1 after 30-days of maturation (~19.73 ± 2.27 MPa), and the lowest σ_c was observed for C-TA5 after 1-day of maturation (~7.23 ± 1.17 MPa). No significant differences were observed between σ_c of C-TA0, C-TA1 and C-TA2 at any of the time points ($P > 0.05$) while C-TA3, C-TA4 and C-TA5 all demonstrated significantly lower σ_c when compared to C-TA0 ($P < 0.05$). Moreover, at 1-day, C-TA4 and C-TA5 showed significantly lower σ_c compared to C-TA3 ($P < 0.05$), however at 7- and 30-days, no differences were observed between these three GPCs ($P > 0.05$).

Figure 4(b) displays σ_b as a function of Ga content and time. C-TA0 demonstrated the greatest σ_b after 30-days of maturation (~8.19 ± 0.55 MPa) while C-TA5 demonstrated the lowest σ_b after 1-day of maturation
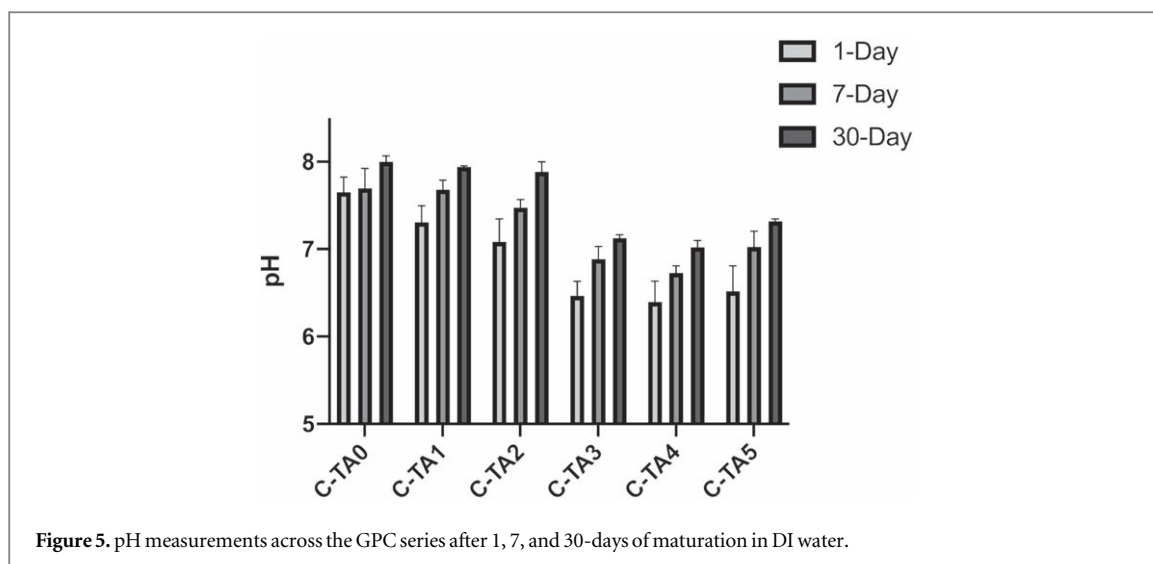
Figure 5. pH measurements across the GPC series after 1, 7, and 30-days of maturation in DI water.

($\sim$4.07 $\pm$ 0.14 MPa). Overall, no significant differences were observed between the σ_b of C-TA0 and C-TA1 at any time point ($P > 0.05$). Furthermore, C-TA2, C-TA3, C-TA4 and C-TA5 all demonstrated significantly lower σ_b than C-TA0 and C-TA1 at both 1- and 7-day time points ($P < 0.05$). However, at 30-days, no differences were observed between C-TA1, C-TA2, C-TA3 and C-TA4 ($P > 0.05$), and the σ_b of C-TA5 was observed to be significantly lower than all other GPCs ($P < 0.05$).

The modulus (E) of each GPC was calculated from the stress-strain curve obtained during the determination of compressive strength. Figure 4(c) displays E as a function of Ga concentration and time. C-TA0 demonstrated the greatest E after 7-days of maturation ($\sim$144 $\pm$ 16 MPa), while C-TA5 demonstrated the lowest E after 1-day of maturation ($\sim$41 $\pm$ 3.6 MPa). No significant differences were observed between C-TA0, C-TA1 and C-TA2 at 1-day ($P > 0.05$), while C-TA3, C-TA4 and C-TA5 were significantly lower than C-TA0 and C-TA1 ($P < 0.05$). At 7-days, the E of all the GPCs containing Ga were significantly lower than C-TA0 ($P < 0.05$). However, by 30-days, no significant differences were observed between C-TA0, C-TA1, C-TA2 and C-TA3 ($P > 0.05$), while C-TA4 and C-TA5 demonstrated a significantly lower E compared to the other four GPCs ($P < 0.05$).

The results of the σ_c and σ_b are in agreement with the results reported in previous studies [59, 60], which reported a decrease in these mechanical properties with the incorporation of Ga in their respective GPC series; although, both of the previous studies noticed an increase in the mechanical properties from their 8-to-16 mol% Ga GPC. The current study demonstrates that 1–2 mol% Ga incorporation does not affect this GPC's mechanical properties, while $\geqslant$ 3 mol% Ga causes deleterious effects. Moreover, a comparison of E values suggests that C-TA0 matures faster, demonstrating no significant increase from 7- to 30-days ($P = 0.0823$), while the GPCs with Ga demonstrated a gradual increase in E through each maturation point (aside from C-TA1, which demonstrated a slight decrease from 1-day to 7-days), all showing significant differences between 7- and 30-day samples ($P < 0.05$). This trend would follow the principle that a reduction in glass reactivity would decrease cross-linking between the glass cations and the PAA chains [73].

Furthermore, this trend may also be explained by the theory of entangled polymer dynamics discussed in section 3.3. [70]. If the difference in molecular diameter and electronegativity between Zn and Ga results in an increased bond length between the polymer chains, then the consequent increase in average tube diameter (a) would also increase the number of Kuhn monomers in a single entanglement stand (N_E) (equation (3)). Furthermore, if the total number of Kuhn monomers in a single polymer chain is represented by N, then the total number of entanglements is taken as the ratio of N_E/N. As N_E increases, the number of total entanglements experienced by a single polymer strand would decrease and result in deleterious effects on the cement's mechanical properties.

3.6. pH analysis

The pH of the GPC series is presented in figure 5. No significant differences were observed between the pH of C-TA0 and C-TA1 after 1-day of maturation, and no significant differences were observed between C-TA0, C-TA1 and C-TA2 after 7 and 30-days of maturation ($P > 0.05$). In contrast, C-TA3, C-TA4 and C-TA5 all demonstrated a significantly lower pH compared to C-TA0, C-TA1 and C-TA2 at all time points ($P < 0.05$). Moreover, no differences were observed between C-TA3 and C-TA4 at any time point. At 7-days and 30-days, C-TA4 demonstrated a significantly lower pH compared to C-TA3 and C-TA5 ($P < 0.05$). Overall, two trends were observed: (1) an increase in pH with time, (2) a general decrease in pH with increasing Ga content. The first
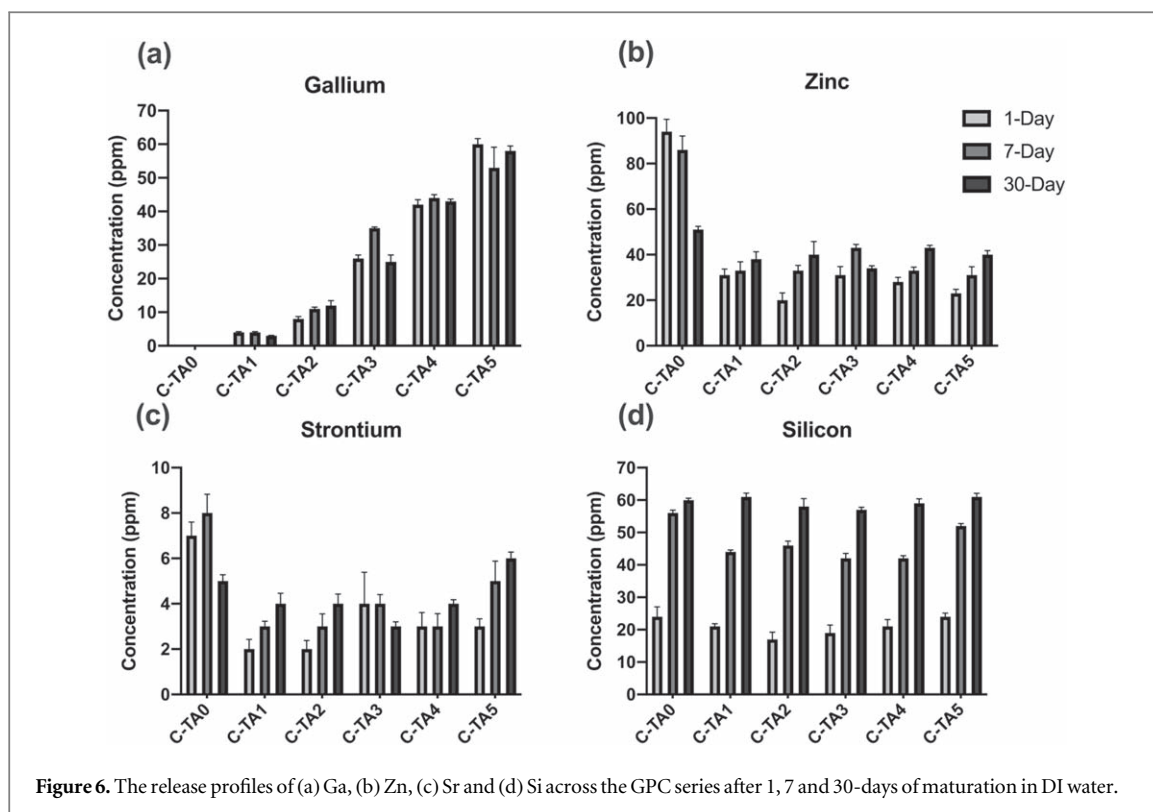
Figure 6. The release profiles of (a) Ga, (b) Zn, (c) Sr and (d) Si across the GPC series after 1, 7 and 30-days of maturation in DI water.

trend follows suit with the continuous maturation of the GPCs. When the glass is exposed to aqueous PAA, the hydrogen ions (H^+) attack the glass structure and liberate cations that bond to the PAA chains. Therefore, as this process continues, the total number of free H^+ decreases, resulting in increased pH [61, 73]. Moreover, the general decrease in pH with increasing Ga content demonstrates an increase in free H^+, implying a decrease in glass reactivity and PAA cross-linking as discussed in section 3.3.

3.7. Ion release

The ion release properties were investigated to understand the effect of Ga incorporation on the solubility of the GPC series. Furthermore, the ion release properties of GPCs are important since the concentration of eluted ions play an essential role in their therapeutic properties. The release profiles of Ga, Zn, Sr and Si were studied only due to their content in the precursor glasses and their therapeutic potential in clinical applications. Figure 6 displays their ion release profiles over 1, 7 and 30 days. In general, the release profiles for each GPC increased over time.

The Ga release profiles (figure 6(a)) demonstrate a controlled release of Ga across the GPC series, ranging from 0–60 ppm. Moreover, the Ga release increased significantly between each GPC at seven and 30-days ($P < 0.05$). Alhalawani *et al* [59] noted a similar trend in Ga release with increasing Ga content. However, this trend could only achieve a maximum release of ∼3 ppm after 30-days of incubation, which is attributed to their relatively lower Ts (∼250 s) [59]. In contrast, the Ts of this GPC series is much longer (33–96 min) and therefore allows for greater levels of Ga mobility/release before complete crosslinking occurs to the set cement. C-TA1 demonstrated the lowest Ga release (other than the control) after 30-days of incubation (∼3 ppm), and C-TA5 demonstrated the largest release after 1-day of incubation (∼60 ppm). The GPC series in the present study presents a wide range of Ga release, which may be used to evaluate chemotherapeutic potential and alterations to bone metabolism.

The Zn release profiles across the GPC series (figure 6(b)) are of particular importance since Zn represents the majority of the precursor glass compositions (table 1). Furthermore, Zn possesses anti-bacterial properties and its elution may regulate the occurrence of postoperative infection [53, 75–77]. The Zn release of C-TA0 was significantly greater than all other GPCs at each of the time points ($P < 0.05$), suggesting that Zn release decreases with the immediate incorporation of Ga ($\geqslant$ 1 mol% Ga) and could be explained by a decrease of glass reactivity with Ga incorporation. Since Zn is the primary cation present in the glass series, it may be responsible for the majority of cross-linking between the PAA chains. Therefore, a decrease in Zn ion release could represent a decrease in their cross-linking between the PAA chains with the inclusion of Ga. However, the Zn release across the five Ga-containing GPCs remains relatively unchanged across the series. Similar results were observed with the Sr elution profile (figure 6(c)), where C-TA0 was found to be significantly higher than all other GPCs after 1 and 7-days ($P < 0.05$); furthermore, the Sr elution from C-TA0 remained significantly higher than C-TA1,

C-TA2, C-TA3 and C-TA4 after 30-days maturation. In-depth IR studies during the initial setting period would be required to investigate further the role of Ga, Zn and Sr in the cements setting chemistry.

The Si release profiles are displayed in figure 6(d). The leaching of ions from the glass leaves an ion-depleted silica gel layer around unreacted glass particles [74], and therefore, Si^{4+} elution may provide evidence of glass reactivity. No significant differences were observed at 1 and 30-days, however the elution of Si of C-TA0 was significantly higher than all other glasses after 7-days of elution ($P < 0.05$), suggesting that Ga containing GPCs mature at a slower rate.

4. Conclusion

This study investigated the substitution of Ga at the expense of Zn (dopant levels ranging from 0%–5%) on an ionomer silicate glass. These studies expand on the current knowledge of Ga-incorporated GPCs. Previous studies [59, 60] demonstrated the synthesis and analysis of two Ga-loaded GPCs (8 and 16 mol%, at the expense of Zn). GPCs loaded with ⩾3 mol% of Ga demonstrated similar results to the previous studies [59, 60], showing increased rheological properties and decreased mechanical properties. These phenomena have been discussed by the difference in elemental properties between Ga and Zn and entangled polymer dynamics using Edward's Tube concept [70]. Furthermore, an analysis of pH confirmed that it decreased with increasing Ga content, suggesting increasing glass network stability leading to decreased reactivity. Finally, the ion release profiles demonstrated a controlled release of Ga across the GPC series, which should prove an advantage in future works when analyzing their dose dependent cytotoxic effects on healthy bone and cancer cells.

Data availability statement

The data that support the findings of this study are available upon reasonable request from the authors.

Disclosure

The authors declare that they have no competing interests.

ORCID iDs

Sunjeev Phull ⬤ https://orcid.org/0000-0003-0752-6243
Alireza Rahimnejad Yazdi ⬤ https://orcid.org/0000-0003-1277-8584
Mark R Towler ⬤ https://orcid.org/0000-0003-1655-1483

References

[1] Dorfman H D and Czerniak B 1995 Bone cancers *Cancer.* **75** 203–10
[2] Key Statistics for Bone Cancer, (n.d.). https://cancer.org/cancer/bone-cancer/about/key-statistics.html (accessed February 22, 2021)
[3] Macedo F, Ladeira K, Pinho F, Saraiva N, Bonito N, Pinto L and Gonçalves F 2017 Bone metastases: an overview *Oncol. Rev.* **11** 43–9
[4] Treating Specific Bone Cancers, (n.d.). https://cancer.org/cancer/bone-cancer/treating/treating-specific-bone-cancers.html (accessed June 2, 2020)
[5] Surgery for Bone Cancer, (n.d.). https://cancer.org/cancer/bone-cancer/treating/surgery.html (accessed June 2, 2020)
[6] Menendez L R, Ahlmann E R, Kermani C and Gotha H 2006 Endoprosthetic reconstruction for neoplasms of the proximal femur *Clin. Orthop. Relat. Res.* **450** 46–51

[7]   Henrichs M-P, Krebs J, Gosheger G, Streitbuerger A, Nottrott M, Sauer T, Hoell S, Singh G and Hardes J 2014 Modular tumor endoprostheses in surgical palliation of long-bone metastases: a reduction in tumor burden and a durable reconstruction *World J. Surg. Oncol.* **12** 330

[8]   Bernthal N M, Schwartz A J, Oakes D A, Kabo J M and Eckardt J J 2010 How long do endoprosthetic reconstructions for proximal femoral tumors last? *Clin. Orthop. Relat. Res.* **468** 2867–74

[9]   Asavamongkolkul A, Waikakul S, Phimolsarnti R, Kiatisevi P and Wangsaturaka P 2007 Endoprosthetic reconstruction for malignant bone and soft-tissue tumors *J. Med. Assoc. Thai.* **90** 706–17

[10] Bickels J, Wittig J C, Kollender Y, Henshaw R M, Kellar-Graney K L, Meller I and Malawer M M 2002 Distal femur resection with endoprosthetic reconstruction *Clin. Orthop. Relat. Res.* **400** 225–35

[11] Qadir I, Umer M and Baloch N 2012 Functional outcome of limb salvage surgery with mega-endoprosthetic reconstruction for bone tumors *Arch. Orthop. Trauma Surg.* **132** 1227–32

[12] Wafa H, Reddy K, Grimer R, Abudu A, Jeys L, Carter S and Tillman R 2015 Does total humeral endoprosthetic replacement provide reliable reconstruction with preservation of a useful extremity? *Clin. Orthop. Relat. Res.* **473** 917–25

[13] Wedin R and Bauer H C F 2005 Surgical treatment of skeletal metastatic lesions of the proximal femur *J. Bone Joint Surg. Br.* **87-B** 1653–7

[14] Benevenia J, Kirchner R, Patterson F, Beebe K, Wirtz D C, Rivero S, Palma M and Friedrich M J 2016 Outcomes of a modular intercalary endoprosthesis as treatment for segmental defects of the femur, tibia, and humerus *Clin. Orthop. Relat. Res.* **474** 539–48

[15] Habermann E T, Sachs R, Stern R E, Hirsh D M and Anderson W J 1982 The pathology and treatment of metastatic disease of the femur *Clin. Orthop. Relat. Res.* **169** 70–82

[16] Bernthal N M, Hegde V, Zoller S D, Park H Y, Ghodasra J H, Johansen D, Eilber F, Eilber F C, Chandhanayingyong C and Eckardt J J 2018 Long-term outcomes of cement in cement technique for revision endoprosthesis surgery *J. Surg. Oncol.* **117** 443–50

[17] Jeys L M, Grimer R J, Carter S R and Tillman R M 2003 Risk of amputation following limb salvage surgery with endoprosthetic replacement, in a consecutive series of 1261 patients *Int. Orthop.* **27** 160–3

[18] Sharma S, Turcotte R E, Isler M H and Wong C 2007 Experience with cemented large segment endoprostheses for tumors *Clin. Orthop. Relat. Res.* **459** 54–9

[19] Wirganowicz P Z, Eckardt J J, Dorey F J, Eilber F R and Kabo J M 1999 Etiology and results of tumor endoprosthesis revision surgery in 64 patients *Clin. Orthop. Relat. Res.* **358** 64–74

[20] Phull S S, Yazdi A R, Ghert M and Towler M R 2020 A review of the use of bone cement in orthopedic oncology and the potential for local chemotherapeutic drug treatment *J. Bone Oncol.* **26** 100345

[21] Hernigou P, Thiery J, Benoit J, Voisin M, Leroux P, Hagege G, Delepine G and Goutallier D 1989 Methotrexate diffusion from acrylic cement. Local chemotherapy for bone tumours *J. Bone Joint Surg. Br.* **71-B** 804–11

[22] Prochazka E, Soukup T, Hroch M, Fuksa L, Brcakova E, Cermanova J, Kolouchova G, Urban K, Mokry J and Micuda S 2010 Methotrexate released *in vitro* from bone cement inhibits human stem cell proliferation in S/G2 phase *Int. Orthop.* **34** 137–42

[23] Draenert F G and Draenert K 2008 Methotrexate-loaded polymethylmethacrylate bone cement for local bone metastasis therapy: pilot animal study in the rabbit patellar groove *Chemotherapy* **54** 412–6

[24] Decker S, Winkelmann W, Nies B and Van Valen F 1999 Cytotoxic effect of methotrexate and its solvent on osteosarcoma cells *in vitro* *J. Bone Jt. Surg.* **81** 545–51

[25] Otsuka M, Matsuda Y, Suwa Y, Fox J L and Higuchi W I 1994 A novel skeletal drug delivery system using a self-setting calcium phosphate cement. 5 drug release behavior from a heterogeneous drug-loaded cement containing an anticancer drug *J. Pharm. Sci.* **83** 1565–8

[26] Otsuka M, Matsuda Y, Fox J L and Higuchi W I 1995 A novel skeletal drug delivery system using self-setting calcium phosphate cement. 9: effects of the mixing solution volume on anticancer drug release from homogeneous drug-loaded cement *J. Pharm. Sci.* **84** 733–6

[27] Tahara Y and Ishii Y 2001 Apatite cement containing cis-diamminedichloroplatinum implanted in rabbit femur for sustained release of the anticancer drug and bone formation *J. Orthop. Sci.* **6** 556–65

[28] Tani T, Okada K, Takahashi S, Suzuki N, Shimada Y and Itoi E 2006 Doxorubicin-loaded calcium phosphate cement in the management of bone and soft tissue tumors *In Vivo* **20** 55–60

[29] Tanzawa Y, Tsuchiya H, Shirai T, Nishida H, Hayashi K, Takeuchi A, Tomita K and Kawahara M 2011 Potentiation of the antitumor effect of calcium phosphate cement containing anticancer drug and caffeine on rat osteosarcoma *J. Orthop. Sci.* **16** 77–84

[30] Yang Z, Li D, Han J, Li J, Li X, Li Z and Li S 2009 Incorporation of methotrexate in calcium phosphate cement: behavior and release *in vitro* and *in vivo* *Orthopedics* **32** 27

[31] Li D, Yang Z, Li X, Li Z, Li J and Yang J 2010 A histological evaluation on osteogenesis and resorption of methotrexate-loaded calcium phosphate cement *in vivo* *Biomed. Mater.* **5** 025007

[32] Kiri L, Filiaggi M and Boyd D 2016 Methotrexate-loaded glass ionomer cements for drug release in the skeleton: an examination of composition-property relationships *J. Biomater. Appl.* **30** 732–9

[33] Hart M M and Adamson R H 1971 Antitumor activity and toxicity of salts of inorganic group IIIa metals: aluminum, gallium, indium, and thallium *Proc. Natl Acad. Sci.* **68** 1623–6

[34] Chitambar C, Matthaeus W, Antholine W, Graff K and O'Brien W 1988 Inhibition of leukemic HL60 cell growth by transferrin-gallium: effects on ribonucleotide reductase and demonstration of drug synergy with hydroxyurea [see comments] *Blood* **72** 1930–6

[35] Chitambar C R, Wereley J P and Riaz-ul-Haq 1994 Synergistic inhibition of T-lymphoblastic leukemic CCRF-CEM cell growth by gallium and recombinant human alpha-interferon through action on cellular iron uptake *Cancer Res.* **54** 3224–8

[36] Myette M S, Elford H L and Chitambar C R 1998 Interaction of gallium nitrate with other inhibitors of ribonucleotide reductase: effects on the proliferation of human leukemic cells *Cancer Lett* **129** 199–204

[37] Hata Y, Sandler A, Loehrer P J, Sledge G W and Weber G 1994 Synergism of taxol and gallium nitrate in human breast carcinoma cells: schedule dependency *Oncol. Res.* **6** 19–24

[38] Cazzola M, Bergamaschi G, Dezza L and Arosio P 1990 Manipulations of cellular iron metabolism for modulating normal and malignant cell proliferation: achievements and prospects *Blood* **75** 1903–19

[39] Larson S M, Rasey J S, Allen D R, Nelson N J, Grunbaum Z, Harp G D and Williams D L 1980 Common pathway for tumor cell uptake of gallium-67 and iron-59 via a transferrin receptor *JNCI J. Natl. Cancer Inst.* **64** 41–53

[40] Reichard P and Ehrenberg A 1983 Ribonucleotide reductase–a radical enzyme *Science (80-.)*. **221** 514–9

[41] Warrell R P, Bockman R S, Coonley C J, Isaacs M and Staszewski H 1984 Gallium nitrate inhibits calcium resorption from bone and is effective treatment for cancer-related hypercalcemia *J. Clin. Invest.* **73** 1487–90

[42] Warrell R P, Alcock N W and Bockman R S 1987 Gallium nitrate inhibits accelerated bone turnover in patients with bone metastases *J. Clin. Oncol.* **5** 292–8

[43] Warrell R P, Murphy W K, Schulman P, O'Dwyer P J and Heller G 1991 A randomized double-blind study of gallium nitrate compared with etidronate for acute control of cancer-related hypercalcemia *J. Clin. Oncol.* **9** 1467–75

[44] Cvitkovic F, Armand J-P, Tubiana-Hulin M, Rossi J-F and Warrell R P 2006 Randomized, double-blind, phase II trial of gallium nitrate compared with pamidronate for acute control of cancer-related hypercalcemia *Cancer J* **12** 47–53

[45] Chitambar C R 2010 Medical applications and toxicities of gallium compounds *Int. J. Environ. Res. Public Health.* **7** 2337–61

[46] Chen D A and Arriaga M A 2003 Technical refinements and precautions during ionomeric cement reconstruction of incus erosion during revision stapedectomy *Laryngoscope.* **113** 848–52

[47] Powis D R, Follerås T, Merson S A and Wilson A D 1982 Improved adhesion of a glass ionomer cement to dentin and enamel *J. Dent. Res.* **61** 1416–22

[48] Celik H, Aslan Felek S, Islam A, Demirci M, Samim E and Oztuna D 2009 The impact of fixated glass ionomer cement and springy cortical bone incudostapedial joint reconstruction on hearing results *Acta Otolaryngol* **129** 1368–73

[49] Blades M C, Moore D P, Revell P A and Hill R 1998 *In vivo* skeletal response and biomechanical assessment of two novel polyalkenoate cements following femoral implantation in the female New Zealand White rabbit *J. Mater. Sci. Mater. Med.* **9** 701–6

[50] Boyce B F, Elder H Y, Elliot H L, Fogelman I, Fell G S, Junor B J, Beastall G and Boyle I T 1982 Hypercalcaemic osteomalacia due to aluminium toxicity *Lancet* **320** 1009–13

[51] Khader B, Peel S and Towler M 2017 An injectable glass polyalkenoate cement engineered for fracture fixation and stabilization *J. Funct. Biomater.* **8** 25

[52] Alhalawani A M and Towler M R 2017 A novel tantalum-containing bioglass. Part I. Structure and solubility *Mater. Sci. Eng.* C **72** 202–11

[53] Alhalawani A M, Mehrvar C, Stone W, Waldman S D and Towler M R 2017 A novel tantalum-containing bioglass. Part II. Development of a bioadhesive for sternal fixation and repair *Mater. Sci. Eng.* C **71** 401–11

[54] Mehrvar C, Kuzyk P, Shamlou J, Safir O, Zalzal P, Alhalawani A, Towler M R and Papini M 2019 Novel adhesives for distal radius fixation: a biomechanical analysis *J. Mech. Behav. Biomed. Mater.* **89** 99–106

[55] Wren A W, Boyd D, Thornton R, Cooney J C and Towler M R 2009 Antibacterial properties of a tri-sodium citrate modified glass polyalkenoate cement *J. Biomed. Mater. Res. - Part B Appl. Biomater.* **90B** 700–9

[56] Dickey B T, Kehoe S and Boyd D 2013 Novel adaptations to zinc-silicate glass polyalkenoate cements: the unexpected influences of germanium based glasses on handling characteristics and mechanical properties *J. Mech. Behav. Biomed. Mater.* **23** 8–21

[57] Clarkin O M, Boyd D, Madigan S and Towler M R 2009 Comparison of an experimental bone cement with a commercial control, Hydroset™ *J. Mater. Sci. Mater. Med.* **20** 1563–70

[58] Boyd D, Clarkin O M, Wren A W and Towler M R 2008 Zinc-based glass polyalkenoate cements with improved setting times and mechanical properties *Acta Biomater.* **4** 425–31

[59] Alhalawani A, Curran D, Pingguan-Murphy B, Boyd D and Towler M 2013 A novel glass polyalkenoate cement for fixation and stabilisation of the ribcage, post sternotomy surgery: an *ex-vivo* study *J. Funct. Biomater.* **4** 329–57

[60] Wren A W, Coughlan A, Placek L and Towler M R 2012 Gallium containing glass polyalkenoate anti-cancerous bone cements: glass characterization and physical properties *J. Mater. Sci. Mater. Med.* **23** 1823–33

[61] Alhalawani A M F, Curran D J, Boyd D and Towler M R 2016 The role of poly(acrylic acid) in conventional glass polyalkenoate cements *J. Polym. Eng.* **36** 221–37

[62] Kaur G, Pandey O P, Singh K, Homa D, Scott B and Pickrell G 2014 A review of bioactive glasses: their structure, properties, fabrication and apatite formation *J. Biomed. Mater. Res. Part* A **102** 254–74

[63] Hoppe A, Güldal N S and Boccaccini A R 2011 A review of the biological response to ionic dissolution products from bioactive glasses and glass-ceramics *Biomaterials* **32** 2757–74

[64] Zalzal P, Safir O, Alhalawani A, Papini M and Towler M 2018 Percutaneous upper extremity fracture fixation using a novel glass-based adhesive *J. Orthop.* **15** 67–9

[65] International Organization for Standardization 2007 Dentistry-Water-based cements-Part 1: Powder/liquid acid-base cements (ISO 9917-1:2007) https://www.iso.org/standard/45818.html

[66] Williams J A, Billington R W and Pearson G J 2002 The effect of the disc support system on biaxial tensile strength of a glass ionomer cement *Dent. Mater.* **18** 376–9

[67] Musić S, Filipović-Vinceković N and Sekovanić L 2011 Precipitation of amorphous SiO_2 particles and their properties, Brazilian *J. Chem. Eng.* **28** 89–94

[68] Choi M, Kang Y R, Lim I S and Chang Y H 2018 Structural characterization of cellulose obtained from extraction wastes of graviola (annona muricata) leaf *Prev. Nutr. Food Sci.* **23** 166–70

[69] Huh S H 2011 Thermal reduction of graphene oxide *Phys. Appl. Graphene - Exp., Dr Sergey* (Rijeka: InTech) pp 74–90

[70] Doi M and Edwards S 1986 *The Theory of Polymer Dynamics* (Oxford: Clarendon)

[71] Driessen M, Miller T and Grassian V 1998 Photocatalytic oxidation of trichloroethylene on zinc oxide: characterization of surface-bound and gas-phase products and intermediates with FT-IR spectroscopy *J. Mol. Catal. A: Chem.* **131** 149–56

[72] Nicholson J W 1998 Chemistry of glass-ionomer cements: a review *Biomaterials* **19** 485–94

[73] Wilson A D and Nicholson J W 2005 *Acid-Base Cements: Their Biomedical and Industrial Applications* (Cambridge: Cambridge University Press)

[74] Wasson E A and Nicholson J W 1991 Studies on the setting chemistry of glass-ionomer cements *Clin. Mater.* **7** 289–93

[75] Söderberg T A, Sunzel B, Holm S, Elmros T, Hallmans G and Sjöberg S 1990 Antibacterial effect of zinc oxide *in vitro*, Scand *J. Plast. Reconstr. Surg. Hand Surg.* **24** 193–7

[76] Gammoh N Z and Rink L 2017 Zinc in infection and inflammation *Nutrients* **9** 624

[77] Coughlan A, Scanlon K, Mahon B P and Towler M R 2010 Zinc and silver glass polyalkenoate cements: an evaluation of their antibacterial nature *Biomed. Mater. Eng.* **20** 99–106